


 Cite this: *New J. Chem.*, 2018, 42, 13367

 Received 12th May 2018,
 Accepted 25th June 2018

DOI: 10.1039/c8nj02344a

rsc.li/njc

Continuous detection of HCl and NH₃ gases with a high-performance fluorescent polymer sensor†

 Ning Xu,^a Rui-Lei Wang,^a Dong-Peng Li,^a Zi-Yan Zhou,^{id}*^a Tian Zhang,^{*a}
 Yu-Zhong Xie^{*b} and Zhong-Min Su^{id}^c

A novel fluorescent triazine-based covalent organic polymer (COP-1) sensor for HCl and NH₃ gases has been designed and synthesized. Both the COP-1 powders that were dispersed in solvents and the COP-1 film that was formed on the surface of quartz sheets exhibited stable fluorescence and a sensitive HCl/NH₃ response. Immersion in HCl-bubbled solvents weakens and red-shifts the fluorescence emission of the COP-1 powders, owing to a protonation-induced charge transfer (CT). Subsequent injection of NH₃ into the solvents recovers the fluorescence via deprotonation. Interestingly, the microporous COP-1 film also shows a similar fluorescence response to HCl/NH₃ gas, with high sensitivity and good reversibility, which suggests that it could serve as a solid-state optical probe for continuous and quantitative detection of HCl and NH₃ gases. The formation of the red-shifting hydrogen bonds is found to be the origin of the response.

Introduction

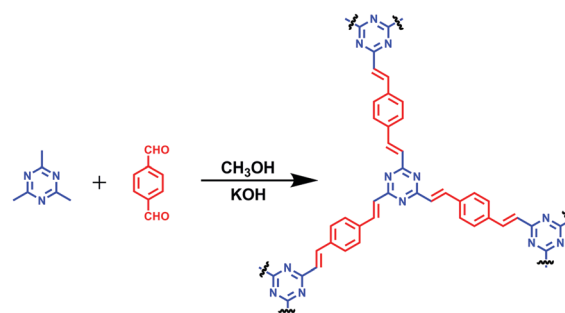
Irritating, volatile and colorless hydrogen chloride (HCl) and ammonia (NH₃) gases are widely found in industry.^{1–4} The main sources of HCl and NH₃ gases in air are fuel burning, and chemical and biological metabolic processes.^{5,6} HCl gas is easily dissolved in water to form hydrochloric acid, which is one ingredient of acid rain.^{7,8} A serious corrosion effect on metals, facilities and buildings is also correlated with HCl and NH₃ gases.⁹ HCl and NH₃ gases can be inhaled into the human body via the respiratory system, and long-term exposure may cause laryngeal mucosal irritation, nasal erosion ulcers and gastrointestinal diseases.^{10,11} In order to mitigate the hazard as much as possible, on-site and real-time monitoring of the pollutants is quite important.^{12–16} Traditional detection methods for HCl and NH₃ gases show deficiencies in sensitivity, selectivity and operation.^{17–19}

Optical detection technology shows the great advantages of high sensitivity, good selectivity, easy operation and low cost,

and so it has been extensively applied in environmental, industrial and biological fields.^{20–22} We are focused on developing well-behaved optical sensors for the detection of HCl and NH₃ gas, and particularly those that can be operated in the solid state.²³

Although several optical sensors for HCl and NH₃ gases have been reported, the solid-state ones with good reversibility and real-time efficiency are still appealing.^{24–27} Recently, Kalimuthu *et al.* reported an optochemical gaseous HCl sensor with a *meso*-tetramesitylporphyrin (MTMP) deposited glass substrate. The Soret band of the MTMP film was shifted from 434 nm to 452 nm upon exposure to HCl gas, whereas no shift was observed when the film was subsequently treated with NH₃ gas.¹² Deshusses *et al.* reported a polyaniline composite membrane for the detection of NH₃ gas. However, it requires at least 30 minutes to complete the sensing process.¹³

In this work, we synthesized a novel triazine-based covalent organic polymer (COP-1) (Scheme 1). The microporous COP-1



Scheme 1 The synthetic route of COP-1.

^a School of Chemistry and Chemical Engineering, Shandong University of Technology, Zibo 255049, People's Republic of China. E-mail: zyzhou@sdu.edu.cn, tzhang@sdu.edu.cn

^b Department of Chemistry, Yanbian University, Yanji 133002, People's Republic of China. E-mail: whyjs@ybu.edu.cn

^c Institute of Functional Material Chemistry, Faculty of Chemistry, Northeast Normal University, Changchun 130024, People's Republic of China

† Electronic supplementary information (ESI) available: PXRD, FT-IR, UV-Vis DSR, VB-XPS, SEM, TGA, fluorescence spectroscopy, fluorescence photo and a picture of the NTO character and transition proportion. See DOI: 10.1039/c8nj02344a

film was formed on the surface of quartz sheets under solvent thermal conditions. The homogeneous pores distributed on the COP-1 film are significant for gas detection. Gratifyingly, the COP-1 film shows strong fluorescence, contrary to usual luminescent materials with aggregation-induced quenching (ACQ) traits.²⁸ Moreover, experimental results show that the COP-1 film could serve as a solid-state probe for HCl/NH₃ gas, which features real-time responses, easy operation, high sensitivity and good reversibility. Quantum chemical calculations were also performed to investigate the detection mechanism.

Experimental

Materials and instruments

Powder X-ray diffraction (XRD) patterns were recorded on a Siemens D5005 diffractometer with Cu K_α ($\lambda = 1.5418 \text{ \AA}$) radiation in the range of 3–50°. Fourier transform infrared (FT-IR) spectra were obtained using a Thermo Nicolet A370 spectrometer (KBr pellets). X-ray photoelectron spectroscopy (XPS) was obtained using an Escalab 250 instrument. The UV-Vis diffuse reflectance spectra (DRS) were recorded on a Shimadzu UV-3600 spectrometer. Scanning electron microscope (SEM) images were obtained using a Quanta FEG250 field emission environmental SEM (FEI, United States). Nitrogen gas and carbon dioxide gas porosimetry measurements were performed on automatic volumetric adsorption equipment (ASIQM0G002-3) and a porosity analyzer after the samples were outgassed under vacuum at 70 °C for 6 h. Thermogravimetric (TGA) curves were measured using a Germany STA449C-QMS403C thermal analyser. The fluorescence spectra were measured using a Tianjin Gangdong F-380 spectrophotometer. Different humidity environments were created using a Constant Temperature and Humidity Chamber (BPHS-060A, Shanghai Bluepard Experimental Instruments Co., Ltd).

All of the chemicals were obtained commercially and used as received unless otherwise stated. Potassium carbonate (K₂CO₃), potassium hydroxide (KOH), methanol (CH₃OH), dichloromethane (CH₂Cl₂), ethanol (CH₃CH₂OH), acetonitrile (CH₃CN), benzene (C₆H₆), sodium chloride (NaCl), acetic acid (CH₃COOH) and NH₃·H₂O were obtained from Kermel Chemical Reagent Co., Ltd (Tianjin, China). Concentrated sulfuric acid (H₂SO₄) and concentrated hydrochloric acid (HCl) were obtained from Sinopharm Chemical Reagent Co., Ltd (Shanghai, China). 1,4-Phthalaldehyde was obtained from Sun Chemical Technology Co., Ltd (Shanghai, China). Deionized water was obtained from a Sartorius 611DI water purification system. 2,4,6-Trimethyl-1,3,5-triazine was prepared according to the literature.²⁹

Synthesis of 2,4,6-trimethyl-1,3,5-triazine

Anhydrous acetonitrile (53 mL, 1 mol), absolute ethanol (58 mL, 1 mol) and anhydrous benzene (82 mL, 1 mol) were put into a 500 mL round-bottom flask, and then HCl gas (43.1 g) was added under stirring. The mixture was stirred at room temperature for 48 h. The solid was collected *via* filtration and was then washed three times (10 mL × 3) with dichloromethane (106.4 g, 86.1%).

The solid (61.75 g, 0.5 mol, dissolved in 100 mL dichloromethane) and K₂CO₃ (86 g, 0.6 mol, dissolved in 300 mL distilled water) were rapidly mixed and stirred for 10 min. The organic phase was separated and the aqueous phase was extracted twice (30 mL × 2) with dichloromethane. The organic phase was dried over anhydrous K₂CO₃. The fractions below 60 °C were removed *via* distillation to get a pale yellow liquid (acetimide ethyl ester, 36.7 g, 83.7%).

Acetic acid (3 mL, 0.063 mol) was slowly added into acetimide ethyl ester (67.9 g, 0.78 mol) under stirring, and the reaction temperature was maintained between 25–30 °C. Then the mixture was stirred for 24 h. After completion of the reaction, the fractions below 80 °C were removed *via* distillation, and the residue was diluted with an appropriate amount of methylene chloride. The white solid was removed *via* pumping filtration. The filtrate was distilled at atmospheric pressure, and the fractions between 149–155 °C were collected (15.7 g, 16%).

Synthesis of COP-1

2,4,6-Trimethyl-1,3,5-triazine (0.24 g, 2 mmol), 1,4-phthalaldehyde (0.40 g, 3 mmol), potassium hydroxide (0.33 g, 6 mmol) and methanol (75 mL) were put into a 100 mL Teflon reactor. After the mixture was sonicated for 10 min, the reactor was transferred to an oven, and then heated at 80 °C for 72 h. A yellow precipitate formed, which was collected *via* filtration and then washed with methanol three times. The collected sample was dried at 80 °C under vacuum for 12 h to give a yellow powder (78% isolated yield).

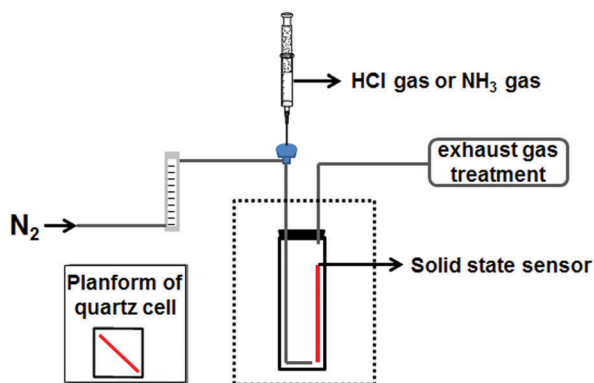
Synthesis of the COP-1 film

A quartz sheet (11.0 mm × 35.0 mm) was immersed into a chromic acid solution at 70 °C for 60 min, and was then washed thoroughly with acetone and ultrapure water.

2,4,6-trimethyl-1,3,5-triazine (0.24 g, 2 mmol), 1,4-phthalaldehyde (0.40 g, 3 mmol), potassium hydroxide (0.33 g, 6 mmol) and methanol (75 mL) were added to a reactor (100 mL). The mixture was sonicated for 10 min, and the quartz sheets were added. The reactor was heated at 80 °C for 72 h until a layer of COP-1 film formed on the surface of the quartz sheet. The prepared COP-1 film was washed with methanol and dried at room temperature.

Experimental procedures for the detection of HCl and NH₃ gases

A homemade device²³ was constructed for the detection of HCl and NH₃ gas (Scheme 2). Gaseous HCl or NH₃ of various concentrations was obtained by injecting a certain volume (0.05 mL, 0.1 mL, 0.15 mL, 0.2 mL or 0.25 mL) of HCl or NH₃ gas into a 4.3 mL sealed cuvette with an airtight syringe. The fluorescence properties of the COP-1 film that was exposed to HCl gas were monitored after leaving it for 5 minutes. Afterwards, excess HCl gas was purged with nitrogen gas, and then we injected sufficient NH₃ gas into the sealed cuvette to recover the film's fluorescence. When the fluorescence of the COP-1 film recovered to its initial state, we purged the excess NH₃ gas and repeated the above procedure for the measurement of another concentration. The COP-1 film used to investigate the

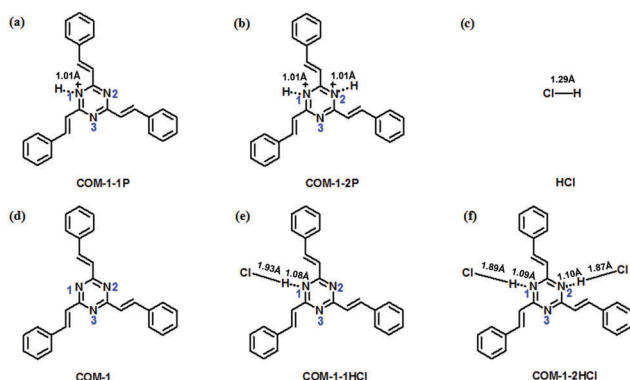


Scheme 2 Device for the detection of HCl and NH₃ gases.

fluorescence response to NH₃ gas was pretreated with abundant HCl gas. The aim was to determine an original state with completely quenched fluorescence intensity. Similarly, the fluorescence properties of the COP-1 film that was exposed to NH₃ gas were monitored after leaving it for 5 minutes. Afterwards, the excess NH₃ gas was purged with nitrogen gas, and we then injected sufficient HCl gas to recover the film's fluorescence. When the fluorescence of the COP-1 film recovered to the original state, we purged the excess HCl gas and repeated the above procedure for the measurement of another concentration. The temperature was 28 °C and the relative humidity was 38% when detecting HCl and NH₃ gases.

Quantum chemical calculations

The monomer model that we used as the effective fragment in calculations for COP-1 was named COM-1. The geometry optimization and frequency calculations were performed using density functional theory (DFT) for the ground states of COM-1-1P, COM-1-2P, HCl, COM-1, COM-1-1HCl and COM-1-2HCl (Scheme 3) at the B3LYP^{30,31} level with a 6-31+G(d) basis set. The local energy minima were ensured *via* the absence of imaginary frequencies and no symmetry constraint was adopted. The electrostatic potential (ESP) and natural bond orbital (NBO) analyses were also conducted at the same level. Geometry and frequency calculations for the excited S₁ states of COM-1-1P and COM-1-2P were



Scheme 3 Computational models for COM-1-1P (a), COM-1-2P (b), HCl (c), COM-1 (d), COM-1-1HCl (e) and COM-1-2HCl (f).

performed using the time-dependent DFT (TD-DFT) approach at the B3LYP/6-31+G(d) level. The excited-state transition properties at the optimized geometries were obtained at the range-separated CAM-B3LYP level with a 6-31+G(d) basis set.³² All of the above calculations were carried out using the Gaussian 09 package.³³

The vibrationally resolved fluorescence spectra, and the radiative (k_r) and internal conversion (k_{ic}) rate constants for COM-1-1P and COM-1-2P were computed using the multimode coupled thermal vibration correlation function (TVCF) formalism³⁴ implemented in the Molecular Materials Property Prediction Package (MOMAP),³⁵ in which the photophysics module shows superiority in predicting the optical properties of polymers and solid-state emitters.³⁶

Results and discussions

Synthesis conditions

The influence of the raw material ratio and the reaction temperature on the yield has been studied. We employed three different raw material ratios and conducted the experiments at three different temperatures. The yields of the obtained products are shown in Table S1 (ESI[†]). The optimal ratio of the raw materials was determined to be 2:3 (2,4,6-trimethyl-1,3,5-triazine: 1,4-phthalaldehyde) and the optimal reaction temperature was determined to be 80 °C.

Structure characterizations

The structure of COP-1 was firstly characterized using powder XRD and FT-IR (Fig. S1 in the ESI[†]). The powder XRD pattern shows two strong peaks, suggesting a semi-crystalline nature.^{37,38} The diffraction peaks at 8.5° and 26.3° can be assigned to the (110) and (001) planes, respectively. The FT-IR spectrum of COP-1 shows a characteristic vibrating band at 1631 cm⁻¹, indicating the existence of an olefin group. Moreover, the band at 1373 cm⁻¹ can be assigned to the triazine ring.

As a powerful tool for evaluating the chemical composition of macromolecules,³⁹ an XPS analysis of COP-1 was performed and the results are shown in Fig. 1 as the total (a) and the deconvoluted high-resolution C 1s (b) and N 1s (c) spectra. The peaks at 284.4 and 284.9 eV on the high-resolution XPS spectrum of C 1s can be assigned to the C-C bond of the benzene ring and the C=C bond, respectively. The peaks at 286.6 and 288.7 eV can be ascribed to the carbon of the triazine ring. For N 1s, the peaks at 398.7 eV and 399.1 eV correspond to the C-N and C=N bonds in the triazine ring, respectively.^{40–42} By combining with the measurements from the room-temperature UV-Vis DRS, we also obtained the band energies and band gap results of COP-1 (Fig. S2 in the ESI[†]). The valence band (VB) energy and band gap were assessed to be 1.14 eV and 2.50 eV, respectively. By simple addition, the conduction band (CB) energy is 3.64 eV.

The morphologies of the COP-1 film were characterized using SEM (Fig. S3 in the ESI[†]). The COP-1 film possesses pores with various sizes, indicating its potential application for adsorption and catalysis. On the surface of the COP-1 film,

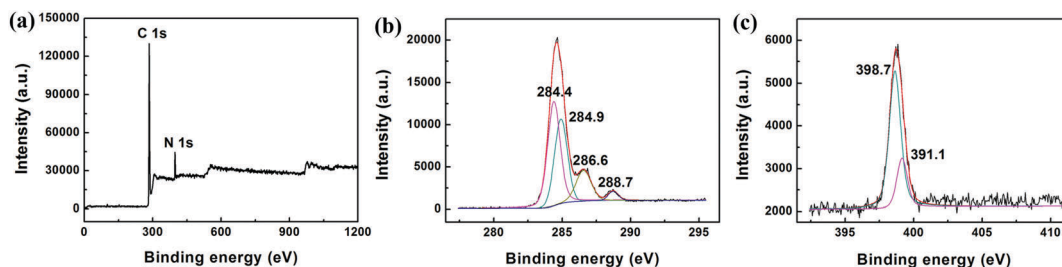


Fig. 1 XPS survey spectrum for COP-1 (a), and the high-resolution parts of the spectra for C 1s (b) and N 1s (c).

homogeneous pores are distributed, revealing its sheet-like structure. The N_2 and CO_2 adsorption assays at low temperatures show sufficient porosity of the COP-1 powders, which further suggests its microcellular polymeric framework (Fig. 2). The aperture size determined from the pore-size distribution curve was 1.4 nm. The Brunauer–Emmett–Teller (BET) surface area was determined to be $29.1 \text{ cm}^2 \text{ g}^{-1}$, and the pore volume was $0.037 \text{ cm}^3 \text{ g}^{-1}$. All of the above results indicate perfect pore distributions.

Thermal and fluorescence stability

As can be seen from the TGA curve, COP-1 shows good thermal stability with a decomposition temperature as high as 450°C and a total weight loss of 50% after decomposition (Fig. S4 in the ESI[†]), indicating that COP-1 is thermally stable. The fluorescence stability of a solid-state optical material has great importance for use in sensing applications. The fluorescence spectra were examined at room temperature as shown in Fig. S5 (ESI[†]). Even after a month, no obvious changes in the band shape and fluorescence intensity were observed for both the COP-1 powders and the COP-1 film, indicating excellent fluorescence stability.

Detection of HCl and NH_3 in liquid medium

The abundant electron-donating nitrogen (N) atoms in COP-1 tend to accept protons, which offers the opportunity for it to be applied as a pH monitor. Therefore, we studied the fluorescence response of the COP-1 powders dispersed in aqueous solution to various pH values (Fig. 3). The results show that the fluorescence intensity declines with gradually decreasing pH values. Particularly, in strongly acidic medium ($\text{pH} < 3$), a significantly weakened and red-shifted emission was observed. It was found that the thermodynamic $\text{p}K_a$ value of the NH^+ moiety at the N atom of the triazine ring fell in the range 2.82–3.30.⁴³ Thus, at least one N atom of the triazine core is protonated when $\text{pH} < \text{p}K_a$.

To gain deeper insight into the pH-dependent luminescence behavior of the COP-1 powders dispersed in acid medium ($\text{pH} < 3$), we performed theoretical calculations on COM-1-1P and COM-1-2P (see Scheme 3). We propose that more of the N atoms of the triazine moiety are protonated as the pH decreases. The calculated vibrationally resolved fluorescence spectra at room temperature are shown in Fig. 4. The fluorescence spectrum of COM-1-2P exhibits a drastic red-shift compared to

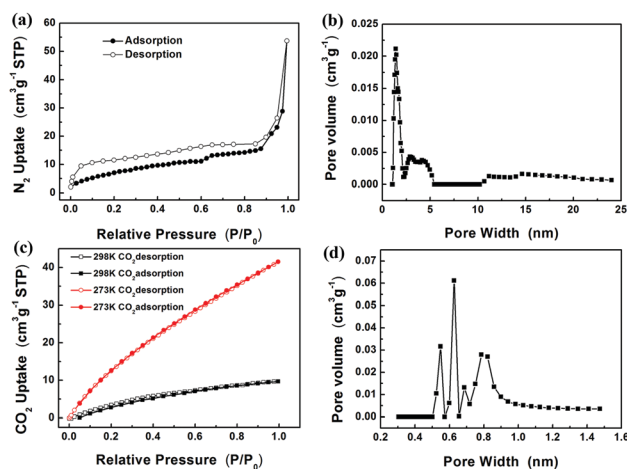


Fig. 2 (a) N_2 adsorption curve at 77 K; (b) pore-size distribution (N_2) curve at 77 K; (c) CO_2 adsorption curves at 273 K and 298 K; (d) pore-size distribution (CO_2) curve at 273 K.

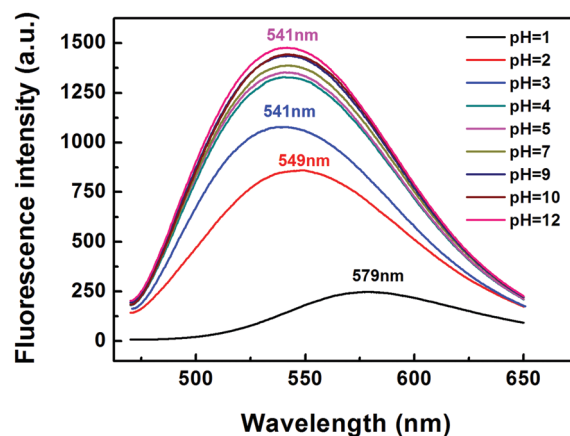


Fig. 3 Fluorescence response of the COP-1 powders dispersed in aqueous solution to various pH values ($\lambda_{\text{max}} = 453 \text{ nm}$).

that of COM-1-1P, whereas the fluorescence intensity declines remarkably, in good agreement with the experimental observations. Moreover, the fluorescence quantum yield $[\Phi_F = k_r/(k_r + k_{ic})]$ predicted *via* computation also shows a decrease from 0.52 for COM-1-1P to 0.20 for COM-1-2P. The weakened emission arises from the k_r value being reduced by more than one order of magnitude, overwhelming the k_{ic} value that was merely reduced fourfold (see Table 1).

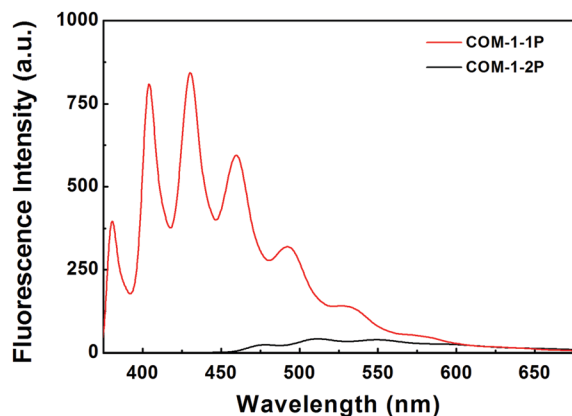


Fig. 4 Calculated vibrationally resolved fluorescence spectra of COM-1-1P and COM-1-2P ($T = 298$ K).

Excited state properties play important roles in determining excited state dynamics. Natural transition orbital (NTO) analyses for the S_1 states were performed and the corresponding landscapes are shown in Fig. S6 (ESI[†]). It can be seen that the S_1 state of COM-1-1P exhibits a hybridized local and charge-transfer (HLCT)⁴⁴ feature, with local excitation (LE) on the upper styryl branch and a charge transfer (CT) from the bottom styryl branch to the central triazine ring. Conversely, an almost pure CT character was found for COM-1-2P, with an obvious CT from the left two styryl branches to the triazine core and the right styryl branch. The HLCT state in COM-1-1P offers an effective pathway for obtaining efficient luminescence, as not only does the LE contribute to a significant orbital overlap to strengthen k_r , but also the CT provides full exciton utilization. However, the relatively pure CT state in COM-1-2P shows orbital separation, which induces a lower k_r value and a red-shifted emission compared to those of COM-1-1P. The calculation results suggest that protonation could promote the intramolecular charge transfer, thus giving rise to the weak and red-shifted emission.

With the aim of investigating the response of the solvent-dispersed COP-1 powders to HCl/NH₃, HCl gas was bubbled through different organic solvents. Fortunately, observable fluorescence changes from green to orange took place in all solvents. Subsequently injecting NH₃ gas into the solvents recovers the fluorescence (Fig. S7 in the ESI[†]). The reason for this can be ascribed to the protonation *via* the dissociation of HCl and the deprotonation upon further contact with NH₃ in liquid, similar to the above-stated pH-dependent luminescence mechanism. As HCl or NH₃ gas cannot be dissolved in organic solvents efficiently, only qualitative results were given to show its sensing ability for HCl/NH₃.

Table 1 Calculated k_r , k_{ic} and Φ_F values ($T = 298$ K) for COM-1-1P and COM-1-2P

| | k_r (s^{-1}) | k_{ic} (s^{-1}) | Φ_F |
|----------|--------------------|-----------------------|----------|
| COM-1-1P | 2.00×10^8 | 1.85×10^8 | 0.52 |
| COM-1-2P | 1.12×10^7 | 0.46×10^8 | 0.20 |

Detection of gaseous HCl and NH₃ using the COP-1 film

Encouraged by its sensing ability in liquid, we endeavored to develop a gaseous HCl/NH₃ sensor with COP-1. As the COP-1 powders are limited in convenient and practical applications, we finally attached them onto quartz sheets to form a polymer film. Sensor experiments were done by first exposing the COP-1 film to HCl gas and then to NH₃ gas. Images of this are shown in Fig. 5. The color of the COP-1 film firstly changes from yellow to orange, and then subsequently recovers to the original colour under visible light. The fluorescence of the COP-1 film changes from greenish yellow to dark orange at first and recovers afterwards under UV light. The structures of the COP-1 powders before and after exposure to HCl gas then to NH₃ gas were also characterized using powder XRD and FT-IR. The major peaks on both the powder XRD patterns and the IR spectra experience slight changes (Fig. S8 in the ESI[†]), indicating that the skeleton of COP-1 was hardly damaged upon exposure to HCl/NH₃ gas.

Theoretical calculations were also conducted on HCl, COM-1, COM-1-1HCl and COM-1-2HCl (Scheme 3) to understand the fluorescence response of the COP-1 film to HCl gas. According to the electrostatic potential (ESP) diagram, the adsorption of HCl molecules (Fig. 6a) to the N atoms of the triazine ring of COM-1 (Fig. 6b) could form red-shifting hydrogen bonds⁴⁵ with H-Cl bond lengthening, since the negative N pulls the positive H closer to it, leading to the polarization of the H-Cl bond (Fig. 6c and d). The natural population analysis (NPA) charges of significant atoms (Scheme 3) obtained *via* NBO analysis are listed in Table 2. The NPA charges of the hydrogen (H) atoms in the HCl molecules of COM-1-1HCl and COM-1-2HCl are nearly equal to those of the bonded protons of COM-1-1P and COM-1-2P. Moreover, the bond lengths of the N...H-Cl hydrogen bonds in COM-1-1HCl and COM-1-2HCl are also similar to those of the N-proton bonds (see Scheme 3). Thus, the adsorption of HCl molecules to the COP-1 film could also enhance the charge transfer during the excited state transition, which weakens and red-shifts the fluorescence intensity. Subsequent exposure to NH₃ gas removes the HCl molecules adsorbed on the COP-1 film and recovers the fluorescence.

Next we quantitatively investigated the fluorescence response of the original COP-1 film to HCl gas of various concentrations (0.0116, 0.0232, 0.0348, 0.0464 and 0.0580, HCl/N₂, v/v). The HCl gas was gradually injected into a 4.3 mL cuvette containing the COP-1 film with an increasing gaseous HCl concentration, and the procedures are detailed in the experimental section. Weakened and red-shifted fluorescence was found (Fig. 7a), and the fluorescence intensities of the COP-1 film decreased linearly with increasing gaseous HCl concentration (Fig. 7b). The detection limit for HCl gas was calculated to be 1.0967×10^{-4} . Similar procedures were applied to study the quantitative fluorescence response of the pre-treated COP-1 film to NH₃ gas of given concentrations. As expected, enhanced and blue-shifted emission was observed (Fig. 7c), and the emission intensities increased proportionally to the rising gaseous NH₃ concentration (Fig. 7d).

The detection limit for NH₃ gas was determined to be 5.8925×10^{-4} . The above results show that the COP-1 film

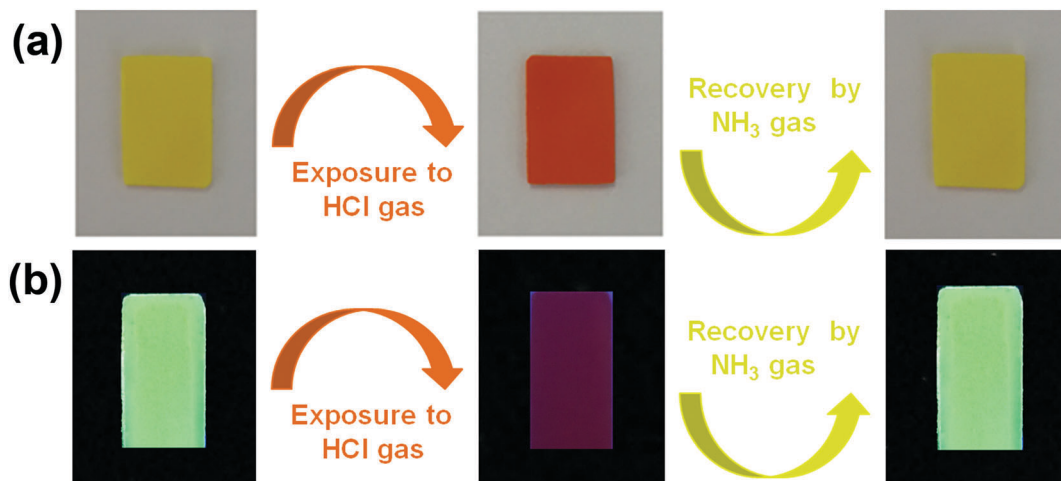


Fig. 5 Images showing the COP-1 film under visible light (a) and UV light (excited at 365 nm) (b) before and after exposure to HCl gas and recovery using NH_3 gas.

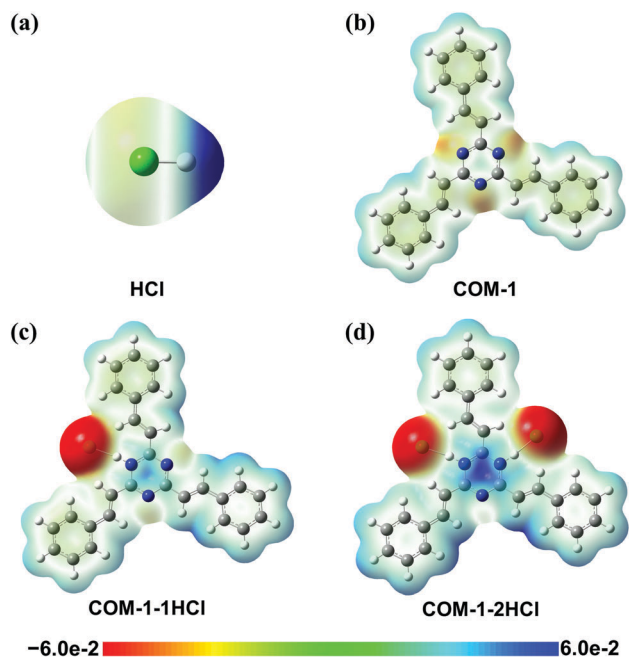


Fig. 6 Electrostatic potential at the 0.002 a.u. isosurface of electron density.

Table 2 NPA charges (in e) on selected atoms for HCl, COM-1 and four complexes obtained using NBO analysis

| | N1 | N2 | N3 | H1 | H2 | Cl1 | Cl2 |
|------------|--------|--------|--------|-------|-------|--------|--------|
| HCl | | | | 0.282 | | -0.282 | |
| COM-1 | -0.515 | -0.516 | -0.515 | | | | |
| COM-1-1HCl | -0.569 | -0.513 | -0.516 | 0.440 | | -0.773 | |
| COM-1-2HCl | -0.573 | -0.572 | -0.510 | 0.435 | 0.432 | -0.747 | -0.743 |
| COM-1-1P | -0.570 | -0.495 | -0.501 | 0.450 | | | |
| COM-1-2P | -0.570 | -0.567 | -0.491 | 0.463 | 0.463 | | |

could be applied for the continuous and quantitative detection of HCl and NH_3 gases with high sensitivity. Reversibility is an

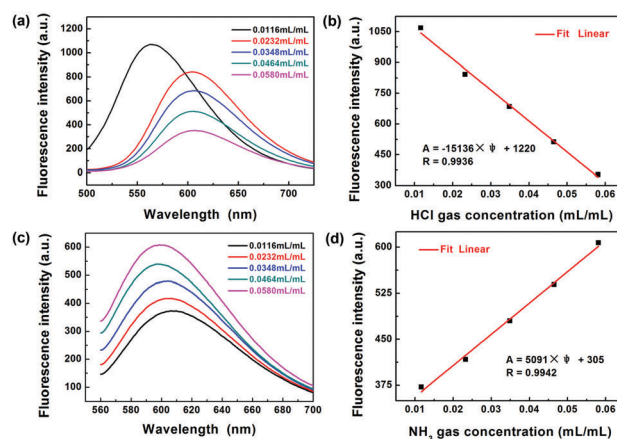


Fig. 7 (a) Fluorescence responses of the original COP-1 film to HCl gas of various concentrations ($\lambda_{\text{max}} = 453 \text{ nm}$); (b) linear relationship between the fluorescence intensities and the gaseous HCl concentration; (c) fluorescence responses of the pretreated COP-1 film to NH_3 gas; (d) linear relationship between the fluorescence intensities and the gaseous NH_3 concentration.

important factor for fluorescent chemosensors in practical applications. The reversibility of the COP-1 film was investigated by cycling the reaction of the probe with HCl and NH_3 gases (Fig. 8), due to the high affinity of NH_3 toward HCl. These reversible fluorescence cycles of bright green to weak orange and back could be repeated five or more times under the same conditions, demonstrating the good reversibility of the COP-1 film toward HCl and NH_3 gases. In addition, we also studied the fluorescent sensor stability of the COP-1 film (Fig. S9 in the ESI†). The experimental results show that there was no significant change in the fluorescence intensity of the COP-1 film after three hours, indicating its good detection stability.

Moreover, we created different humidity environments (40%, 50%, 60%, 70% and 80%) using a Constant Temperature and Humidity Chamber to study the effect of humidity on the detection of HCl gas by COP-1 (Fig. S10 in the ESI†). The cuvette

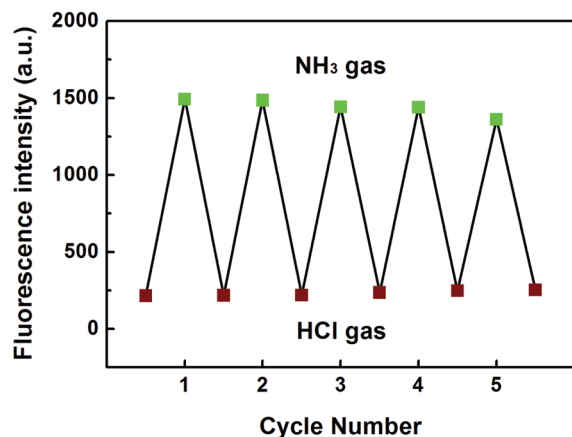


Fig. 8 Fluorescence of the COP-1 film upon alternating treatment with HCl and NH_3 gases.

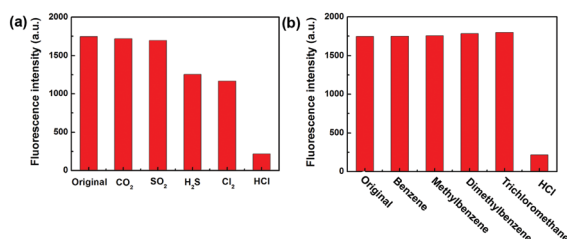


Fig. 9 Responses of the COP-1 film toward other potential co-existing interference gases: (a) acid gases and (b) volatile organic compounds.

containing the COP-1 film was placed in the Constant Temperature and Humidity Chamber under a specific humidity for 15 minutes. After that, 0.3 mL of dry HCl gas was injected into the 4.3 mL cuvette, and then the fluorescence intensity was measured. The results revealed that the humidity had almost no influence on the fluorescence intensity of COP-1 when detecting HCl gas.

To examine the responses of the COP-1 film toward other potential co-existing acid gases, we investigated its responses to CO_2 , SO_2 , H_2S and Cl_2 . Upon exposure to CO_2 and SO_2 , no obvious changes in the fluorescence intensity were observed, as shown in Fig. 9a. The presence of H_2S and Cl_2 could result in a small decrease of the fluorescence intensity ($\sim 25\%$). Volatile organic compounds (VOCs) are also important interference gases in some cases, and so four different VOCs (benzene, methylbenzene, dimethylbenzene and trichloromethane) were chosen as interfering gases to verify the effect on the detection of HCl gas by COP-1. Upon exposure to these VOCs, no obvious changes in the fluorescence intensity were observed (Fig. 9b).

Conclusions

In conclusion, we have synthesized a fluorescent triazine-based covalent organic polymer (COP-1) sensor for HCl and NH_3 gases. Both the solvent-dispersed COP-1 powders and the micro-porous COP-1 film exhibited stable fluorescence and a sensitive

HCl/ NH_3 response. The COP-1 powders were used to successively detect HCl and NH_3 in liquid medium. The as-prepared COP-1 film was applied for the reversible detection of HCl and NH_3 gases. Quantum chemical calculations showed that the weak and red-shifted fluorescence response of the COP-1 powders/film to HCl originated from the adsorption of proton/HCl to the N atoms of the triazine rings. The interaction between the negative N of the triazine ring and the positive H of a proton from HCl could lead to a charge-transfer (CT) state. Subsequent exposure of the HCl-pretreated COP-1 powders/film to NH_3 caused deprotonation/desorption and recovered the fluorescence. As a visible and easy-operating detection strategy, this paves a new way for the continuous detection of acidic and alkaline gases.

Conflicts of interest

There are no conflicts to declare.

Acknowledgements

This work is supported by the Natural Science Foundation of Shandong Province (Grant No. ZR2017BB034 and ZR2018LB019) and the National Natural Science Foundation of China (Grant No. 21703122 and 21463026). Thanks is given for the support of the Scientific Research Foundation of Shandong University of Technology.

Notes and references

- 1 J. Thornton, J. Kercher, T. Riedel, N. Wagner, J. Cozic, J. Holloway, W. Dube, P. Quinn, A. Middlebrook, B. Alexander and S. Brown, *Nature*, 2010, **464**, 271.
- 2 N. B. Shustova, A. F. Cozzolino, S. Reineke, M. Baldo and M. Dinca, *J. Am. Chem. Soc.*, 2013, **135**, 13326.
- 3 J. Geltmeyer, G. Vancoillie, I. Steyaert, B. Breyne, G. Cousins, K. Lava, R. Hoogenboom, K. Buysse and K. Clerck, *Adv. Funct. Mater.*, 2016, **26**, 5987.
- 4 C. W. Zhao, J. P. Ma, Q. K. Liu, X. R. Wang, Y. Liu, J. Yang, J. S. Yang and Y. B. Dong, *Chem. Commun.*, 2016, **52**, 5238.
- 5 C. Q. Yin, G. T. Duan and W. P. Cai, *RSC Adv.*, 2016, **6**, 103185.
- 6 M. E. Genovese, E. Colusso, M. Colombo, A. Martucci, A. Athanassiou and D. Fragouli, *J. Mater. Chem. A*, 2017, **5**, 339.
- 7 P. Muthukumar and S. A. John, *Sens. Actuators, B*, 2011, **159**, 238.
- 8 X. C. Li, C. Y. Wang, Y. Wan, W. Y. Lai, L. Zhao, M. F. Yin and W. Huang, *Chem. Commun.*, 2016, **52**, 2748.
- 9 M. Matsuguchi and T. Asahi, *Sens. Actuators, B*, 2011, **160**, 999.
- 10 M. Shahabuddin, A. Sharma, J. Kumar, M. Tomar, A. Umar and V. Gupta, *Sens. Actuators, B*, 2014, **194**, 410.
- 11 M. Matsuguchi, K. Takaoka and H. Kai, *Sens. Actuators, B*, 2015, **208**, 106.
- 12 P. Kalimuthu and S. Abraham John, *Anal. Chim. Acta*, 2008, **627**, 247.

- 13 T. Zhang, S. Mubeen, B. Yoo, N. V. Myung and M. A. Deshusses, *Nanotechnology*, 2009, **20**, 255501.
- 14 D. Li, Y. Zhang, Z. Fan and J. Yu, *Chem. Commun.*, 2015, **51**, 13830.
- 15 A. Rengaraj, P. Puthiaraj, Y. Haldorai, N. S. Heo, S. K. Hwang, Y. K. Han, S. Kwon, W. S. Ahn and Y. S. Huh, *ACS Appl. Mater. Interfaces*, 2016, **8**, 8947.
- 16 H. Wei, S. Chai, N. Hu, Z. Yang, L. Wei and L. Wang, *Chem. Commun.*, 2015, **51**, 12178.
- 17 B. Timmer and W. Olthuis, *Sens. Actuators, B*, 2005, **107**, 666.
- 18 X. Chen, H. W. Hu, Z. M. Xia, W. Gao, W. Y. Gou, Y. Q. Qu and Y. Y. Ma, *J. Mater. Chem. C*, 2017, **5**, 309.
- 19 M. Hu, W. M. Kang, Y. X. Zhao, J. Shi and B. W. Cheng, *RSC Adv.*, 2017, **7**, 26849.
- 20 Q. F. Li, L. Jin, L. L. Li, W. P. Ma, Z. L. Wang and J. H. Hao, *J. Mater. Chem. C*, 2017, **5**, 4670.
- 21 M. Matsuguchi and A. Tada, *Sens. Actuators, B*, 2017, **251**, 821.
- 22 Y. Zhang, S. Li, G. Pan, H. Yang, M. Qile, J. Chen, Q. Song and D. Yan, *Sens. Actuators, B*, 2018, **254**, 785.
- 23 Y. Z. Xie, G. G. Shan, Z. Y. Zhou and Z. M. Su, *Sens. Actuators, B*, 2013, **177**, 41.
- 24 Y. Zhan, P. Yang, G. Li, Y. Zhang and Y. Baoa, *New J. Chem.*, 2017, **41**, 263.
- 25 L. Tao, F. Niu, D. Zhang, T. Wang and Q. Wang, *New J. Chem.*, 2014, **38**, 2774.
- 26 A. Das and D. M. D'Alessandro, *Dalton Trans.*, 2016, **45**, 6824.
- 27 F. Niu, L. Tao, Y. Deng, Q. Wang and W. Song, *New J. Chem.*, 2014, **38**, 2269.
- 28 Y. Cui, Y. Liu, J. Liu, J. Du, Y. Yu, S. Wang, Z. Liang and J. Yu, *Polym. Chem.*, 2017, **8**, 4842.
- 29 Y. Z. Cui, Q. Fang, G. Xue, W. T. Yu, H. Lei and Z. Q. Liu, *Acta Chim. Sin.*, 2003, **61**, 307.
- 30 C. Lee, W. Yang and R. G. Parr, *Phys. Rev. B: Condens. Matter Mater. Phys.*, 1988, **37**, 785.
- 31 A. BecNe, *J. Chem. Phys.*, 1993, **98**, 5648.
- 32 T. Yanai, D. P. Tew and N. C. Handy, *Chem. Phys. Lett.*, 2004, **393**, 51.
- 33 M. J. Frisch, G. W. Trucks, H. B. Schlegel, G. E. Scuseria, M. A. Robb, J. R. Cheeseman, G. Scalmani, V. Barone, G. A. Petersson, H. Nakatsuji, X. Li, M. Caricato, A. Marenich, J. Bloino, B. G. Janesko, R. Gomperts, B. Mennucci, H. P. Hratchian, J. V. Ortiz, A. F. Izmaylov, J. L. Sonnenberg, D. Williams-Young, F. Ding, F. Lipparini, F. Egidi, J. Goings, B. Peng, A. Petrone, T. Henderson, D. Ranasinghe, V. G. Zakrzewski, J. Gao, N. Rega, G. Zheng, W. Liang, M. Hada, M. Ehara, K. Toyota, R. Fukuda, J. Hasegawa, M. Ishida, T. Nakajima, Y. Honda, O. Kitao, H. Nakai, T. Vreven, K. Throssell, J. A. Montgomery, Jr., J. E. Peralta, F. Ogliaro, M. Bearpark, J. J. Heyd, E. Brothers, K. N. Kudin, V. N. Staroverov, T. Keith, R. Kobayashi, J. Normand, K. Raghavachari, A. Rendell, J. C. Burant, S. S. Iyengar, J. Tomasi, M. Cossi, J. M. Millam, M. Klene, C. Adamo, R. Cammi, J. W. Ochterski, R. L. Martin, K. Morokuma, O. Farkas, J. B. Foresman and D. J. Fox, *Gaussian 09, Revision D.01*, Gaussian, Inc., Wallingford, CT, 2009.
- 34 Y. Niu, Q. Peng, C. Deng, X. Gao and Z. Shuai, *J. Phys. Chem. A*, 2010, **114**, 7817.
- 35 Z. G. Shuai, Q. Peng, Y. L. Niu and H. Geng, *MOMAP, a molecular materials property prediction package, Revision 0.2.004*, Tsinghua University, Beijing, China, 2014, <http://www.shuaigroup.net/>.
- 36 Z. G. Shuai and Q. Peng, *Phys. Rep.*, 2014, **537**, 123.
- 37 T. Wang, D. Huang, Z. Yang, S. Xu, G. He, X. Li, N. Hu, G. Yin, D. He and L. Zhang, *Nano-Micro Lett.*, 2016, **8**, 95.
- 38 L. Hao, J. Ning, B. Luo, B. Wang, Y. Zhang, Z. Tang, J. Yang, A. Thomas and L. Zhi, *J. Am. Chem. Soc.*, 2015, **137**, 219.
- 39 C. Ornelas, J. Broichhagen and M. Weck, *J. Am. Chem. Soc.*, 2010, **132**, 3923.
- 40 B. Asadi, I. Mohammadpoor-Baltork, S. Tangestaninejad, M. Moghadam, V. Mirkhani and A. Landarani-Isfahani, *New J. Chem.*, 2016, **40**, 6171.
- 41 M. Can, M. Doğan, M. İmamoğlu and M. Arslan, *React. Funct. Polym.*, 2016, **109**, 151.
- 42 Y. Wu, Z. He, X. Zeng, T. Ren, E. De Vries and E. van der Heide, *Tribol. Int.*, 2017, **109**, 140.
- 43 D. Geffertová, S. T. Ali, V. Šolínová, M. Krečmerová, A. Holý, Z. Havlas and V. Kašíčka, *J. Chromatogr. A*, 2017, **1479**, 185.
- 44 W. Li, Y. Pan, L. Yao, H. Liu, S. Zhang, C. Wang, F. Shen, P. Lu, B. Yang and Y. Ma, *Adv. Opt. Mater.*, 2014, **2**, 892.
- 45 J. Joseph and E. D. Jemmis, *J. Am. Chem. Soc.*, 2007, **129**, 4620.